Combined computational and experimental analysis of a complex of ribonuclease III and the regulatory macrodomain protein, YmdB

Samridhdi Paudyal,[1†] Mercedes Alfonso-Prieto,[2†] Vincenzo Carnevale,[1,2] Shiv K. Redhu,[3] Michael L. Klein,[2,3] and Allen W. Nicholson[1,3]*

[1] Department of Biology, Temple University, Philadelphia, Pennsylvania 19122

[2] Institute for Computational Molecular Science, Temple University, Philadelphia, Pennsylvania 19122

[3] Department of Chemistry, Temple University, Philadelphia, Pennsylvania 19122

ABSTRACT

Ribonuclease III is a conserved bacterial endonuclease that cleaves double-stranded(ds) structures in diverse coding and noncoding RNAs. RNase III is subject to multiple levels of control that in turn confer global post-transcriptional regulation. The *Escherichia coli* macrodomain protein YmdB directly interacts with RNase III, and an increase in YmdB amount *in vivo* correlates with a reduction in RNase III activity. Here, a computational-based structural analysis was performed to identify atomic-level features of the YmdB-RNase III interaction. The docking of monomeric *E. coli* YmdB with a homology model of the *E. coli* RNase III homodimer yields a complex that exhibits an interaction of the conserved YmdB residue R40 with specific RNase III residues at the subunit interface. Surface Plasmon Resonance (SPR) analysis provided a K_D of 61 n*M* for the complex, corresponding to a binding free energy (ΔG) of -9.9 kcal/mol. YmdB R40 and RNase III D128 were identified by *in silico* alanine mutagenesis as thermodynamically important interacting partners. Consistent with the prediction, the YmdB R40A mutation causes a 16-fold increase in K_D ($\Delta\Delta G = +1.8$ kcal/mol), as measured by SPR, and the D128A mutation in both RNase III subunits (D128A/D128$'$A) causes an 83-fold increase in K_D ($\Delta\Delta G = +2.7$ kcal/mol). The greater effect of the D128A/D128$'$A mutation may reflect an altered RNase III secondary structure, as revealed by CD spectroscopy, which also may explain the significant reduction in catalytic activity *in vitro*. The features of the modeled complex relevant to potential RNase III regulatory mechanisms are discussed.

INTRODUCTION

Metabolic pathways operate in a highly regulated manner through the coordinated action of multiple enzymes and associated factors. The enzymes typically function in the context of multisubunit assemblies, often with specific subcellular locations, and are subject to regulation in response to diverse inputs. The maturation and decay of bacterial RNA is accomplished through the action of multiple endoribonucleases and $3'\rightarrow5'$ exoribonucleases.[1–3] The endonucleolytic cleavage of double-stranded (ds) RNA is a prominent aspect of bacterial RNA metabolic pathways. The enzyme responsible for this reaction is ribonuclease III (RNase III), which is a homodimeric phosphodiesterase that requires a divalent metal ion, preferably Mg^{2+}, to cleave duplex structures, providing product termini with 2-nt, $3'$-overhangs.[4,5] RNase III

†Samridhdi Paudyal and Mercedes Alfonso-Prieto contributed equally to this work

*Correspondence to: Allen W. Nicholson, Department of Biology, Temple University, 1900 N. 12th Street, Philadelphia, PA 19122. E-mail: anichol@temple.edu (or) malfonsoprieto@gmail.com

participates in the maturation of diverse cellular, viral, and plasmid transcripts. A primary substrate is the ribosomal(r) RNA precursor, whose cotranscriptional cleavage by RNase III provides the immediate precursors to the mature 16S and 23S rRNAs.[6] RNase III also is involved in RNA turnover, as it provides the initial, rate-determining step in the decay pathways of a number of transcripts.[7] Given its site-selective action on specific substrates, in contrast to a general or subordinate role in RNA formation and breakdown, RNase III has been implicated in regulating gene networks. In this manner, RNase III action influences phenotypes such as virulence, antibiotic production, and phage strategies of infection.[4,5,8]

RNase III is subject to regulation at multiple levels. The relatively low abundance of the enzyme (several hundred molecules in *Escherichia coli*[9]) is established in part through negative autoregulation as a result of RNase III cleavage of its mRNA.[10,11] RNase III catalytic activity is stimulated by phosphorylation during infection by bacteriophage T7. Phosphorylation is catalyzed by the T7-encoded protein kinase and serves to enhance the catalytic capacity of the limited amount of enzyme, thereby allowing optimal maturation of the abundant phage mRNA precursors.[12] RNase III also can be regulated through noncovalent interactions. Kim *et al.* reported that elevated levels of the *E. coli* protein YmdB, occurring either by ectopic overexpression or during cold shock, is accompanied by a decrease in RNase III activity.[13] Coimmunoprecipitation and chemical crosslinking[13] established a physical interaction of YmdB and RNase III. Based on the chemical crosslinking results, Kim *et al.* proposed that YmdB forms a heterodimer with the RNase III polypeptide.[13] While these results indicate that YmdB interacts with RNase III, and that binding affects RNase III activity, the molecular details of the RNase III-YmdB complex and the mechanism of regulation remain unclear.

The YmdB polypeptide is conserved in the Bacteria and contains a macrodomain fold that binds ADP-ribose (ADPR) and related structures.[14,15] *E. coli* YmdB hydrolyzes O-Acetyl-ADP-ribose (OAADPR),[16] which is a product of sirtuin action on lysine-acetylated proteins, and involves NAD^+ as cosubstrate. In *E. coli*, CobB protein functions as a sirtuin.[17] The conservation of YmdB thus may reflect its involvement in protein acetylome regulation, through the processing of NAD^+-related metabolites. A global regulatory role in cell behavior is suggested for YmdB, as the protein has been shown to influence biofilm formation.[18] Given these roles, the YmdB-RNase III interaction suggests a physical as well as functional link between cellular metabolic state and RNase III action. A structural characterization of the YmdB-RNase III interaction would allow definition of a functional interface that connects post-transcriptional regulation with cell behavior. We present here a computational-based analysis of the YmdB-RNase III interaction that was then subjected to experimental evalu-ation. The implications of the interaction in the mechanism of RNase III regulation by YmdB are discussed.

MATERIALS AND METHODS

Materials

Double distilled water was used in all experiments. Molecular biology grade chemicals and reagents were purchased from Sigma-Aldrich or Fisher Scientific. Ni^{2+}-NTA chromatography resin and thrombin cleavage capture kits were purchased from EMD-Millipore. Superdex 10/300 GL columns for AKTA FPLC were purchased from GE Healthcare Life Sciences. Protein assay kits and protein markers for SDS-PAGE were purchased from Bio-Rad Laboratories. Amicon spin concentrators were purchased from EMD-Millipore. Plasmid MiniPrep Kits were purchased from Qiagen, and Biacore-Sensor Chip NTA and buffers used in surface plasmon resonance (SPR) analyses were purchased from GE Healthcare Life Sciences.

Protein mutagenesis and purification

Escherichia coli (*Ec*)-RNase III and *Ec*-YmdB were purified in hexahistidine(H6)-tagged form from recombinant pET-15b plasmid-bearing *E. coli* cells, as described in the Supporting Information (SI; see SI-2).[19] The D128A and R40A mutations were introduced into *Ec*-RNase III and *Ec*-YmdB, respectively, also as described in SI-2.

SPR analysis

SPR was performed with a Biacore 2000 system, using a sensor chip NTA charged with Ni^{2+} ion, and with H6-*Ec*-YmdB or R40A mutant as the immobilized species. *Ec*-RNase III, with the H6-tag enzymatically removed (see SI-3) was the injected analyte. The alternative use of RNase III as the immobilized species was not considered, as the homodimeric protein would carry two H6 tags, creating two attachment points per enzyme that could potentially hinder function. The RNase III-YmdB interaction was measured in terms of Response Units (RU). An amount of *Ec*-YmdB was immobilized on the surface that provided ∼300 RU; then different concentrations of *Ec*-RNase III were injected and the RU recorded. The kinetic "simultaneous k_a/k_d" method of the BIAevaluation software (4.1.1.exe) was used for data fitting and to determine the dissociation constant ($K_D = k_a/k_d$) for the complex. Further experimental details are provided in the Figure 4 legend and Supporting Information Figure SI-3.

Circular dichroism (CD) spectroscopic analysis

The secondary structures of *Ec*-RNase III and *Ec*-YmdB, and the corresponding mutant proteins were

analyzed by CD spectroscopy using a JASCO Model J-815 CD Spectrometer. Spectra (195–250 nm) were recorded at room temperature in 150 mM sodium phosphate (pH 7.5) buffer, at a protein concentration of ~15 µg/mL. Samples were scanned continuously (50 nm/min), with sensitivity set at 100 mdeg; a data pitch of 0.1 nm; a one second response; and a bandwidth of 1 nm.

Homology modeling of *Ec*-RNase III

Three homology models of *Ec*-RNase III were generated, using as templates the available crystal structures of *Aquifex aeolicus* (*Aa*) and *Thermotoga maritima* (*Tm*) RNases III. These structures have been proposed to reflect different steps of the catalytic cycle.[20] The single *Tm*-RNase III structure (PDB entry 1O0W, 2.0 Å resolution) is an RNA- and divalent-metal-ion-free ("apo") form of the enzyme, while the two *Aa*-RNase III structures correspond to the enzyme bound to dsRNA in two alternative modes. In one structure (PDB entry 2NUE, 2.9 Å resolution), the dsRNA is bound to a single dsRNA-binding domain (dsRBD). This structure may reflect an early step in substrate recognition, or "precatalytic" complex.[20] The second structure (PDB entry 2NUG, 1.7 Å resolution) contains two dsRNAs that are bound to the homodimeric RNase III domain (RIIID)[4] and are the products of cleavage of a longer dsRNA. This complex reflects the presence of the Mg^{2+} cofactor in the crystallization buffer and therefore may correspond to a "postcatalytic" complex.[20] The RIIID structures of the *Aa*-RNase III (PDB entries 2NUE and 2NUG) and *Tm*-RNase III (PDB entry 1O0W) templates are essentially identical (the backbone RMSD with respect to the 2NUG structure is 1.31 Å for 2NUE and 1.84 Å for 1O0W). In contrast, the dsRBDs adopt different relative positions ("closed," "partially closed," or "open," for the 2NUG, 2NUE, and 1O0W structures, respectively).[21]

A sequence alignment of the three RNase III polypeptide sequences was inferred from a profile Hidden Markov model (HMM), generated with JackHmmer.[22] We used the *Ec*-RNase III polypeptide sequence as query, and searched iteratively the RefSeq protein database for similar sequences (E-value < 0.01). Supporting Information Figure S1 (SI-1) shows the alignment as visualized with ESPript,[23] as well as the secondary structure of *Ec*-RNase III as predicted by PSIPRED.[24] The *Ec*-RNase III sequence identity is 35 and 34% with the *Tm*-RNase III and *Aa*-RNase III templates, respectively, whereas the sequence identity between the two templates is 37%. The sequence similarity between *Ec*-RNase III and *Tm*-RNase III is 55 and 57% for *Aa*-RNase III, while the similarity of the two templates is 57%. Therefore, the quality of the resulting homology models is expected to be in the medium-to-high range.[25] The predicted C$_\alpha$ RMSD of the model with respect to the native structure (calculated using ModEval)[26] is 2.68 Å for the *Tm*-based model and 2.60 Å for the *Aa*-based models. Modeller (version 9.10)[27,28] was used for pairwise structure-sequence alignment and homology model building, and representative models were selected using the g_cluster tool of the Gromacs package.[29,30] Further details on the homology modeling protocol are provided in SI-1. The three *Ec*-RNase III homology models are shown in Supporting Information Figure S2, SI-1.

Protein-protein docking

Haddock (version 2.0)[31,32] along with CNS (version 1.2)[33,34] was used to obtain a structural model of the RNase III-YmdB complex, using the homology models of Ec-RNase III (see above) and the crystal structure of Ec-YmdB (PDB entry 1SPV, 2.0 Å resolution). We note that previous studies have shown that the use of a homology model for one of the interacting partners does not diminish the reliability of the protein-protein docking model.[35] Specifically, a sequence identity of ~35% (such as the Ec-RNase III homology modeling in this work; see above) is expected to provide near-native models of the protein-protein complex (<3.0 Å interface RMSD).

A blind docking calculation was performed first to determine putative protein interfaces. As this protocol makes no assumptions on the interacting surfaces, no restraining potentials were added to the docking scoring function. The protein structures used were the crystal structure of Ec-YmdB (PDB entry 1SPV) and the 2NUG-based homology model of Ec-RNase III (that is, Ec-RNase III with Mg^{2+}, and dsRNA bound to the catalytic valley). The blind docking protocol and the analysis of the results are described in detail in SI-1.[36–40]

The modeled complex of YmdB and RNase III involving both RIIIDs then was refined by means of restrained docking calculations that included information about the interacting surfaces. In particular, ambiguous interaction restraints (AIRs) were defined between the WHISCY-predicted[41] interface residues of Ec-YmdB (Supporting Information Fig. S3, SI-1) and residues 120–140 of both RIIID subunits of the Ec-RNase III holoenzyme. The 120–140 segment of RNase III had been identified elsewhere to be important for YmdB recognition, based on co-precipitation experiments.[13] The blind docking results (see below) confirmed that this region interacts with YmdB.

Ec-YmdB was docked against all three homology models of Ec-RNase III, to assess the effect on YmdB binding of the specific state of RNase III: "apo" (no dsRNA or metal ion), "pre" (dsRNA bound to the dsRBD), and "post" (cleaved dsRNA bound to the catalytic valley). Also, the use of several homolog template structures as a source of conformational variability has been shown to improve sampling in protein-protein docking.[42] The resulting models were analyzed using a two-step

clustering protocol (see SI-1) to obtain representative structures of the YmdB-RNase III complex for each restrained docking experiment (Fig. 2 and Supporting Information Figs. S10 and S11, SI-1). Additional details of the clustering and analysis of the results are in SI-1.

The restrained docking models of the YmdB-RNase III complex were optimized using a generalized born implicit solvent (GBIS) model,[43] as implemented in NAMD.[44] Further details on the GBIS protocol are provided in SI-1.[45–48] Minimization of the models did not modify significantly the protein-protein interface coming from the docking, but it fixed small backbone deviations resulting from the simulated annealing cycles employed in both the homology modeling and the docking protocols. On minimization, the MolProbity score[49] decreased below 1.5 Å, indicating that steric clashes, rotamer quality, and Ramachandran quality of the complexes are within the average values for X-ray structures of 1.5 Å resolution. Finally, the algorithm Binana[50] (with default parameters), followed by a visual double-check, was used to identify the main protein-protein interactions.

In silico alanine scanning mutagenesis

Computational alanine scanning was performed to identify the RNase III-YmdB interface hot spots. In particular, the analysis was carried out with both the FoldX[51] program and the Robetta[52] webserver, to minimize any possible bias due to the specific force field used. Further details on the alanine scanning calculations can be found in SI-1. Briefly summarized, the interface residues were considered candidate hot spots if both the FoldX and Robetta $\Delta\Delta G_{\text{bind}}$ values were $\geq +1$ kcal/mol.[53] It should be noted that the computational Ala scanning mutates only one of the two equivalent residues of the RNase III dimer (that is, a mutant/wt heterodimer is used in the calculation of $\Delta\Delta G_{\text{bind}}$), whereas the experimental analysis necessarily involves a mutant/mutant homodimer. To address this limitation of the computational methodology, and to be able to compare the results with experimental data, we estimated the change in binding free energy for a given mutant-mutant RNase III homodimer as the sum of the $\Delta\Delta G_{\text{bind}}$ of the two alternative mutant/wt heterodimer forms:

$$\Delta\Delta G_{bind}(XA/X'A) = \Delta\Delta G_{bind}(XA) + \Delta\Delta G_{bind}(X'A) \quad (1)$$

where X and X' are the two symmetry-related RNase III residues, XA and $X'A$ denote the corresponding single alanine mutants, and $XA/X'A$ the double mutant. This additivity approximation[52,54,55] assumes that the two single alanine mutations (XA and $X'A$) are functionally independent, in that the coupling or interaction free energy between the two residues (X and X') is zero. Therefore, the $\Delta\Delta G_{\text{bind}}$ values provided in Table II and in Supporting Information Figure S12 (SI-1) are an esti-mate of the actual values for the mutant/mutant RNase III homodimer.

Sequence analysis of RNase III and YmdB orthologs

Multiple sequence alignments (MSA) of RNase III and YmdB orthologs were generated using BLAST56 followed by refinement with ClustalOmega[57] and visualization using ESPript[23] (Supporting Information Figs. S13 and S17, SI-1). We investigated further the residue conservation in the region of the Ec-RNase III polypeptide (residues 120–140) important for YmdB binding (see Supporting Information Figs. S14 and 15, SI-1).[13] Here, the initial MSA for RNase III was used as a seed to train a HMM using HMMER3.0,[22] which in turn was applied to generate a larger, HMM-based MSA of RNase III sequences (see also SI-1). Sequence logos[58] were generated for the 120–140 region using Weblogo3[59] (see Supporting Information Fig. S13 and SI-1). The sequence insertion in the α6-α7 loop, as observed in the sequence alignment (see also Results), is consistent with the structural alignment using the available RNase III crystallographic structures[20,60] as well as homology models of Ec-RNase III (this work) and Streptomyces coelicolor (Sc) RNase III (obtained from ModBase[61]).

RESULTS

Blind docking calculations

To gain initial insight on the putative interacting surfaces of RNase III and YmdB we performed a blind docking calculation that involved no prior assumptions or information on the interacting surfaces. We used the crystal structure of Ec-YmdB (PDB entry 1SPV) and a structural model of Ec-RNase III, built on the basis of the X-ray structure of Aa-RNase III (PDB entry 2NUG),[20] which contains Mg2+ ions and two dsRNA fragments (resulting from the cleavage of a longer dsRNA) bound in the catalytic valley defined by the RIIID dimer interface.

A center-of-mass (COM) analysis[36,62] of the blind docking results reveals two main interacting regions in Ec-RNase III: one involving both RNase III domains (RIIID and RIIID′), and another involving the dsRNA-binding domain (dsRBD) of each subunit (Fig. 1 and Supporting Information Figs. S4 and S6, SI-1). The first region (represented by clusters 1, 3, and 4 in Fig. 1) is located on the RIIID face opposite from the catalytic valley, and includes residues 120–140 that were shown elsewhere to be important for YmdB recognition.[13] The first binding site corresponds to a complex with YmdB bound to both RNase III subunits, and is named here as the RIIID-YmdB-RIIID′ complex.

A statistical analysis of the protein-protein interface in the blind docking poses[39,40] was used to identify potential interacting residues in the RIIID-YmdB-RIIID′
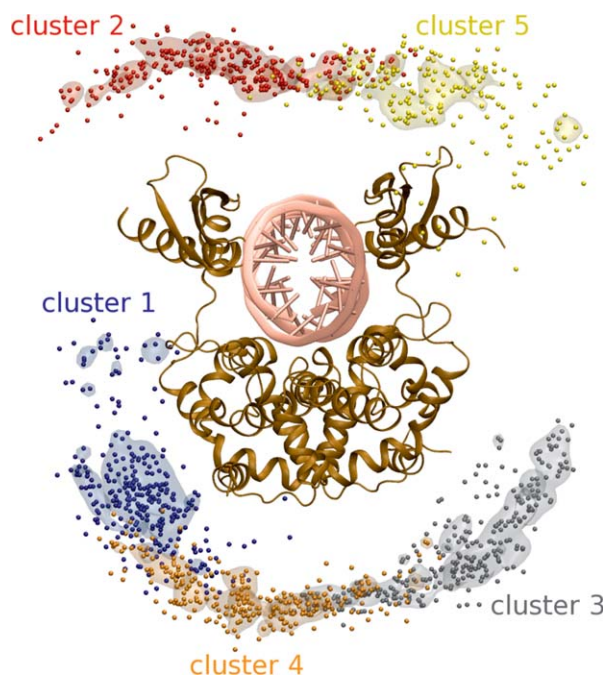
Figure 1

Potential YmdB binding sites on the RNase III surface as obtained by cluster analysis of the blind docking poses. Ec-RNase III is shown in brown cartoon form and the cleaved dsRNA (bound in the catalytic valley) in pink. Shown are the top five Ec-YmdB clusters (representing 35% out of a total of 4000 and ranked according to local density). The small spheres represent the YmdB center of mass (COM), with the color indicating the cluster to which the YmdB docking pose belongs. The number density of each cluster is displayed as a colored isosurface, using the same color code as the corresponding COM subset. The cluster density isovalue is scaled by the number of poses in the cluster (1.3 $\times$ 10 − 4 Å−3 for clusters 1 − 2; 1.4 $\times$ 10 − 4 Å−3 for cluster 3; 1.5 $\times$ 10 − 4 Å−3 for cluster 4; and 1.9 $\times$ 10 − 4 Å−3 for cluster 5).

complex (Supporting Information Figs. S5 and S6, SI-1). For YmdB, the identified residues with the greatest propensity to be at the protein interface are R9, G32, R40, R87, G124, V125, Y126, R130, E161, and E162 (Supporting Information Fig. S5, SI-1). Of these, G32, G124, V125, and Y126 also are located near the postulated ADPR binding site.[16] Interestingly, three of the residues (G32, R40, and Y126) are predicted by WHISCY[41] to be important for protein-protein interactions (Supporting Information Fig. S3, SI-1). For the RIIID (and the symmetry-related RIIID′), five of the ten top residues (R11, Y15, T16, N18, and R59) are located in the N-terminal region of the protein, whereas the other five residues (D128, Q130, K134, N138, and W139) are in the 120–140 segment implicated in YmdB binding[13] (see Supporting Information Figs. S6A and S6B, SI-1).

In addition to the RIIID-YmdB-RIIID′ complex, a second complex was detected in which YmdB interacts with the dsRBDs and the cleaved dsRNA (see clusters 2 and 5 in Fig. 1). The most frequently interacting dsRBD residues are located on the surface that is vicinal to the

cleaved dsRNA (Supporting Information Figs. S6A and S6C, SI-1). While the first complex involving the two RIIIDs is the primary focus in the experiments presented below, the possible functional importance of a second binding site on the dsRBDs, also involving dsRNA, is also considered below (see Discussion).

Restrained docking calculations

We next refined the model of the RIIID-YmdB-RIIID′ complex by means of restrained docking calculations. This approach incorporates information about the interacting surfaces, to confine the conformational search. In particular, we defined AIRs between the WHISCY-predicted interacting residues of YmdB (Supporting Information Fig. S3, SI-1) and the experimentally validated[13] (and rediscovered by blind docking – see above) RIIID residues 120–140. To assess whether the various conformational states of the RNase III structures influence YmdB binding, we docked Ec-YmdB with all three homology models of Ec-RNase III (the apo protein, and the precatalytic and postcatalytic, dsRNA-bound forms – see Materials and Methods).

It should be noted that using both RNase III monomers in the definition of the AIRs biases YmdB docking to the center of the two RIIID subunits. This assumption is based on the blind docking results, showing that (i) YmdB binding simultaneously to both RNase III subunits (that is, formation of RIIID-YmdB-RIIID′ complexes) is more frequent than binding to a single subunit (that is, formation of either RIIID-YmdB or RIIID′-YmdB complexes, without disruption of the RNase III dimer; see Supporting Information Fig. S4, SI-1), and (ii) the residues more frequently found at the RIIID-YmdB interface (D128, Q130, and K134, see Supporting Information Fig. S6, SI-1) are also located at the RIIID-RIIID′ homodimer interface. The validity of this assumption was assessed by performing supplementary restrained docking calculations. First, we performed calculations, using as active residues the amino acids in region 120–140 of only one of the RNase III monomers (RIIID or RIIID′), that would thus bias YmdB docking to a single subunit. The results of this first test show that (i) D128, Q130, and K134, located in between the two RIIIDs, persist as the residues that are more frequently found at the RNase III-YmdB complex interface; (ii) the amount of solvent accessible surface area buried on complex formation decreases, on average, by ∼300 Å^2 when YmdB binds to only one subunit, rather than to both monomers; and (iii) there are fewer RNase III-YmdB interactions across the protein-protein interface in the RIIID-YmdB or RIIID′-YmdB complexes, compared with the RIIID-YmdB-RIIID′ complexes. Therefore, the RIIID-YmdB and RIIID′-YmdB complexes appear to be less stable than the RIIID-YmdB-RIIID′ complexes considered here. Second, we carried out calculations using the amino

acids in region 120–140 of both RNase III monomers (RIIID and RIIID′) as passive residues, rather than as active residues. Since half of the AIRs is discarded at random in each docking trial, YmdB docking is not biased to either subunit. The results of this test show that (i) configurations with YmdB binding to both subunits occur more frequently than those with YmdB binding to a single subunit and (ii) residues located at the RIIID-RIIID′ homodimer interface (D128, Q130, and K134) appear more frequently at the YmdB-RNase III interface. In summary, these results support a model in which YmdB binds at the center of the two interacting RNase III subunits (that is, formation of a RIIID-YmdB-RIIID′ complex). As such, only the restrained docking results, including both RNase III subunits in the definition of the AIRs, were further analyzed.

A COM-based, two-step clustering protocol of the restrained docking results (see SI-1) was used to identify the representative poses of YmdB on the RIIID surface (Supporting Information Figs. S7–S9, SI-1). Similar to the blind docking results, a diverse structural ensemble was obtained. Despite the limited statistics (that is, only 400 poses generated for each restrained docking), the results of the three restrained dockings are similar (panels A and B in Supporting Information Figs. S7–S9, SI-1). The only difference is that, when YmdB binds to apo RNase III, binding to a single subunit is sampled in addition to binding to both subunits, whereas the latter mode is the only one explored when YmdB interacts with RNase III bound to dsRNA. This is most likely due to the different relative positions of the two dsRBDs, which occupy extended (exposed) positions in apo RNase III, but are closed (sequestered) in the dsRNA-bound structures (see Supporting Information Fig. S2, SI-1). As a result, in the apo RNase III complex YmdB is able to establish secondary interactions with the dsRBDs in addition to the primary interaction with the RIIID. Thus, when YmdB binds to a single RIIID subunit in the apo form, the loss of interactions with the other subunit may be compensated by the formation of alternative interactions with the dsRBD of the same monomer. For each of the restrained dockings, the two most populated clusters (blue and red clusters in Supporting Information Figs. S7–S9, SI-1) contains 60–70% of the configurations obtained (see panel C in Supporting Information Figs. S7–S9, SI-1); thus, they could be considered as the main representatives in terms of population. However, since the average Haddock score of the clusters is not significantly different (see Supporting Information Table SI and panel D in Figs. S7–S9, SI-1) we cannot discard any of the clusters with full confidence.

Statistical analysis of the residues found at the protein-protein interface shows that the interfacial frequencies of the YmdB and RNase III residues are similar in the three restrained dockings. The main difference is observed with residues located in the dsRBD (amino acids 155–225) that exhibit nonzero interfacial frequencies in the YmdB-apo RNase III complex, compared with the other two complexes involving RNase III bound to dsRNA. As explained above, this reflects the "open" positions of the dsRBDs in apo RNase III that allow formation of additional contacts with YmdB. The YmdB residues with the greatest interfacial frequency in all three restrained dockings are the G30-G33 tetraglycine segment (98, 100, and 100%, respectively) and R40 (99%), whereas for RNase III the residues are D128 and Q130 (both 99%), followed by K134 (97%). While these interacting residues also were captured in the blind docking, the interfacial frequencies are higher in the restrained docking experiments, due to the use of AIRs that confined the conformational search to the 120–140 region. Nevertheless, it should be noted that of the residues involved in the definition of the AIRs, the interfacial frequency varied from 0 to 100%. This is due to the random removal of half of the AIRs in each docking trial, which effectively compensates for possible false positives in the definition of the restraints, thereby yielding improved docking results.[63]

Figure 2 shows the main representative structure of the RIIID-YmdB-RIIID′ complex obtained through restrained docking of YmdB to RNase III containing dsRNA in the catalytic valley (that is, post-catalytic state). The counterparts for the other two restrained dockings involving the Ec-RNase III apo enzyme, or the dsRNA-bound pre-catalytic state are displayed in Supporting Information Figures S10 and 11 (SI-1). The most distinctive feature of the interface of the complex is YmdB(y) residue R40 that is "anchored" to a "pocket" in RNase III, located in between the RIIID and RIIID′ subunits [Fig. 2(A), and panels A and D in Supporting Information Figs. S10 and S11, SI-1]. Indeed, yR40 is the residue with the largest solvent accessible surface area (SASA) that is buried on complex formation (the change in SASA, ΔSASA, is 83–198 Å^2).[64] Moreover, in all three restrained dockings [Fig. 2(B), and panels B and E in Supporting Information Figs. S10 and S11, SI-1], yR40 is ranked either first or second in terms of the number of interactions with RNase III (Table I and Supporting Information Tables SII and SI-1). A closer examination of the yR40 side-chain [Fig. 2(C) and panels C and F in Supporting Information Figs. S10 and S11, SI-1] reveals that it is encompassed by RNase III residues D128, Q130, E133, and Y50. Thus, the yR40 guanidinium group may engage in salt bridge, hydrogen bond, and/or cation-π interactions.

The interfacial frequencies and YmdB-RNase III interactions listed above provide information about the most probable interacting residues. However, this does not necessarily imply that these residues are the main determinants of complex stability. For example, neighbor amino acids may stabilize an otherwise weak interaction. Therefore, we performed an *in silico* alanine scanning
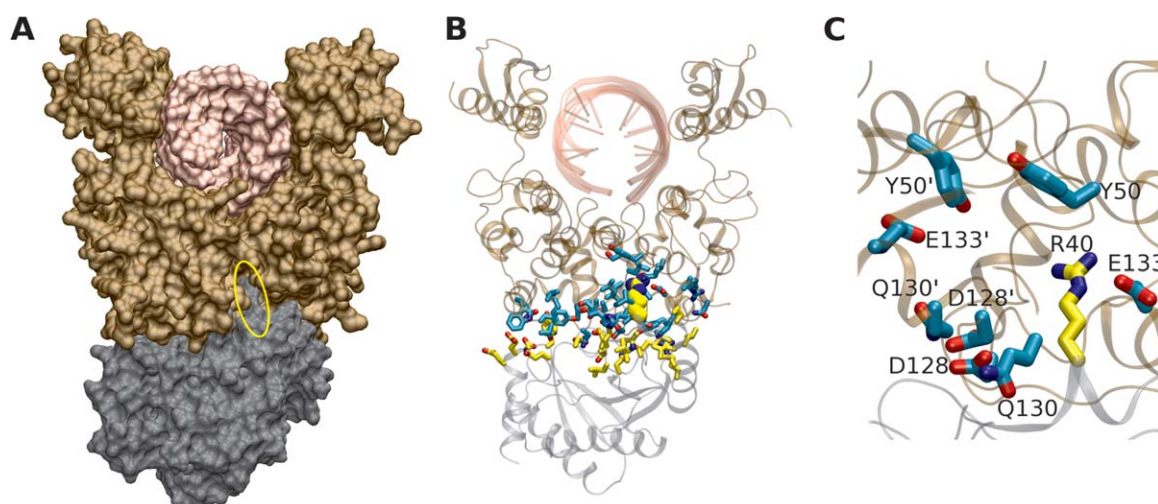
Figure 2

Modeled complex of YmdB and RNase III as obtained by restrained docking. Ec-RNase III is shown bound to cleaved dsRNA in a putative postcatalytic state. (a) Molecular surface of the complex, calculated using a probe of radius 1.4 Å. Ec-YmdB is in gray, RNase III in brown, and the cleaved dsRNA in pink. The position of YmdB R40 at the RNase III dimer interface is highlighted with a yellow ellipse. (**b**) Structure of the complex using a cartoon representation of the proteins with the same color code as in (a). The atomistic details of the interface residues (that is, Those within 4 Å of the complementary partner) are shown as licorice, except for Ec-YmdB R40, which is displayed as spheres. (c) Atoms are in yellow for YmdB and in cyan for RNase III; for both proteins, O atoms are in red, and N atoms are in blue. (c) Close-up of the YmdB-RNase III interface, showing specific residues discussed in the text.

mutagenesis analysis to identify RNase III-YmdB interface "hot spots" (those residues significantly contributing to the binding energy of the complex). Table I (as well as Supporting Information Table SII and Fig. S12, SI-1) provides the calculated $\Delta\Delta G_{bind}$ values. The YmdB residue that is a primary contributor to the binding energy

Table I
Primary Predicted Protein-Protein Interactions and Energetics, Occurring at the Interface of Three Alternative YmdB-RNase III Complexes, and Obtained Through Restrained Docking

YmdB	RNase III (apo)	$\Delta\Delta G_{bind}$ (kcal/mol)	YmdB	RNase III (pre)	$\Delta\Delta G_{bind}$ (kcal/mol)	YmdB	RNase III (post)	$\Delta\Delta G_{bind}$ (kcal/mol)
D11	N18 (hb)	0.0/2.5	D11	N138′ (hb)	0.0/0.1	D11	–	–
T13	L125 (hb)	1.4/1.6	T13	–	–	T13	D126 (hb)	1.3/1.0
K14	D126 (sb)	0.0/0.2	K14	G14′ (hb)	0.9/1.0	K14	H19′ (cp)	0.7/0.1
							L125′ (hc)	
							D126′ (sb)	
S27	L125′ (hb)	0.0/0.4	S27	–	–	S27	D126 (hb)	1.7/2.2
H39	D128′ (sb)	0.9/0.1	H39	–	–	H39	Q130 (hb)	1.3/0.2
R40	I129′ (hb)	2.5/2.5	R40	D128′ (sb)	1.7/3.7	R40	Y50 (cp)	4.4/2.9
							I129′ (hc)	
	E133′ (sb)						E133 (sb)	
D48	K134′ (sb)	0.3/0.0	D48	–	–	D48	–	–
R54	T16′ (hb)	4.9/4.5	R54	–	–	R54	G14 (hb)	1.7/1.1
	D126′ (sb)						Y15 (cp)	
D59	N18′ (hb)	0.6/0.3	D59	–	–	D59	–	–
Y126	–	–	Y126	Y15 (pp)	0.9/0.2	Y126	–	–
Y159	Y15 (pp)	2.0/2.8	Y159	E133′ (hb)	1.3/2.3	Y159	Y15′ (pp)	2.6/3.4
							K134′ (cp)	
	T131 (hb)						N138′ (hb)	
	K134 (hc)						W139′ (pp)	
D160	K134 (sb)	0.2/0.0	D160	H58 (hb)	0.0/0.0	D160	K134′ (sb)	0.0/0.0

Apo denotes the complex of YmdB with the apo form of RNase III; pre, the complex with RNase III in a presumed early step of substrate recognition; and post, the complex with RNase III in a presumed postcatalytic state. Only the representative structure of the first most-populated cluster (that is, blue in Supporting Information Figs. S7–S9, SI-1) is considered in each complex. The YmdB residues interacting with RNase III are ordered according to their position in the sequence, and are matched with the interacting RNase III residue(s). The prime symbols denote interacting residues in the second subunit of the homodimeric holoenzyme. The type of interaction is denoted in parentheses, using the following abbreviations: hb: hydrogen bond; sb: salt bridge; pp: π-π interaction; cp: cation-π interaction; hc: hydrophobic contact. $\Delta\Delta G_{bind}$ is the calculated change in binding free energy of the complex on alanine mutation of the corresponding YmdB residue. Accordingly, interactions involving YmdB backbone atoms are not included. For each interaction, the FoldX value is given first, followed by the corresponding Robetta value.
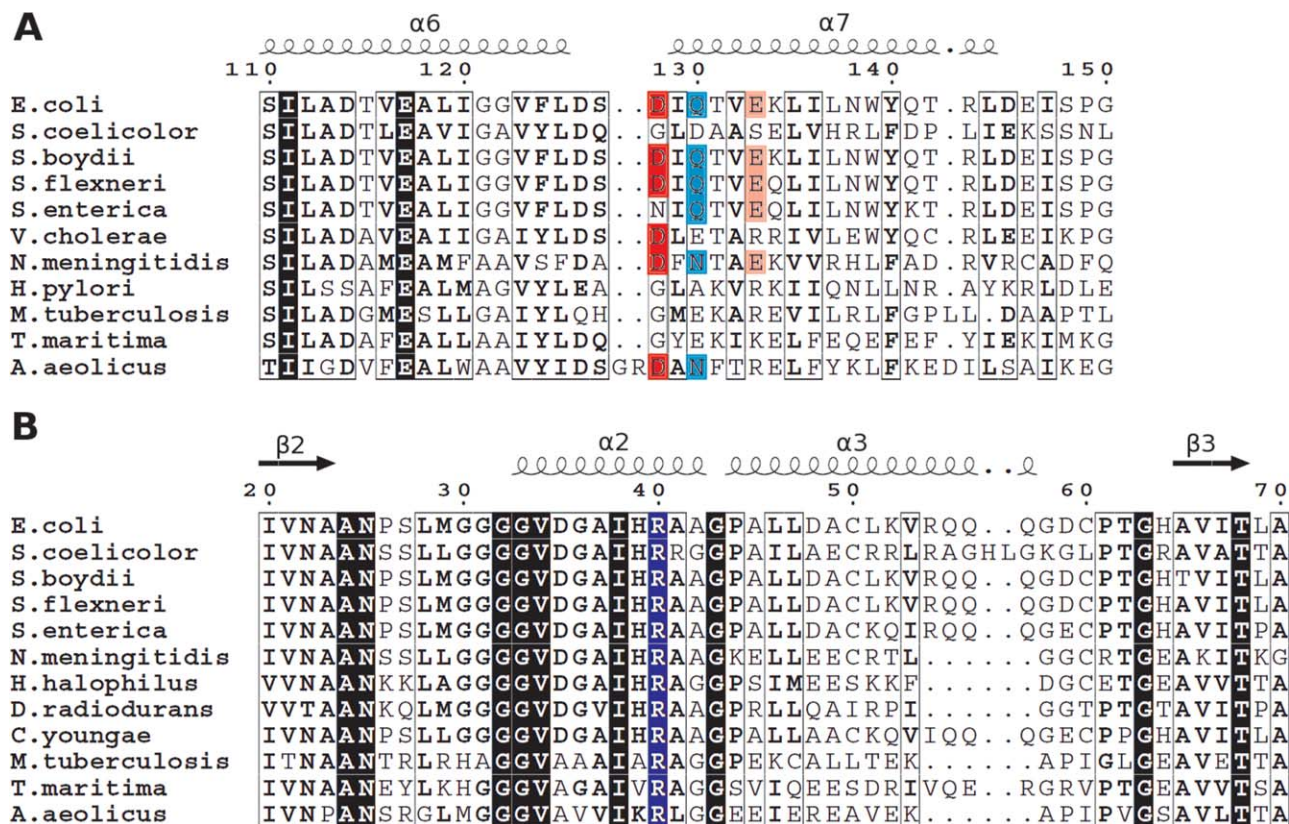
Figure 3

MSA of bacterial orthologs of RNase III (a) and YmdB (b). The residue numbering of Ec-RNase III (a) and Ec-YmdB (b) and the secondary structure elements (predicted using PSIPRED, or obtained from PDB entry 1SPV, respectively) are shown on top. Conserved residues are highlighted in black, and similar residues are boxed. The red- and pink-highlighted residues (D128 and E133 in Ec-RNase III) indicate acidic residues in the proposed YmdB recognition pocket. The cyan-highlighted residues (Q130 in Ec-RNase III) indicate residues predicted to make an intersubunit interaction with D128. The conserved Ec-YmdB residue R40 is highlighted in blue.

is yR40 (Table I and Supporting Information Tables SII and SI-1), followed by yY159 and yR54. For RNase III, only one of the two equivalent residues of the homodimer is mutated to Ala in the computational Ala scanning (that is, a mutant/wt heterodimer is used in the calculation of ΔΔGbind), while the experimental Ala mutagenesis analysis (see next section) necessarily involves a homodimer with a mutation in each subunit. To address this limitation of the calculation, we have estimated the change in binding free energy for a given mutant/mutant homodimer as the sum of the ΔΔGbind of the two alternative mutant/wt heterodimers[52,54,55] [see Eq. (2), SI-1]. Determined in this manner, the ΔΔGbind values (Supporting Information Figs. S12, SI-1) indicate that the main binding energy determinants in RNase III are Q130, D128, and E133, followed by K134.

SPR analysis of the YmdB-RNase III interaction and effect of specific mutations

The restrained docking data was subjected to direct experimental examination, with a focus on the predicted interaction of yR40 with the RIIID recognition pocket that contains D128. In this regard, yR40 (i) has the highest interfacial frequency (99%); (ii) engages in interactions with several RNase III residues (a salt bridge with D128 or E133, a hydrogen bond with I129 or Y50 and/or a cation-π interaction with Y50, see Table I and Supporting Information Table SII and SI-1); (iii) has the highest ΔΔGbind value in the in silico alanine scanning analysis (Table I and Supporting Information Table SII) (in line with Arg, along with Trp and Tyr, as a residue most frequently acting as a hot spot)[65]; and (iv) is conserved among YmdB orthologs [Fig. 3(B)]. For RNase III, potential targets include D128, Q130, or E133. These residues (i) exhibit high interfacial frequencies (99, 99, and 64%, respectively); (ii) interact with yR40 (Table I, and Supporting Information Tables SII and SI-1); and (iii) have high ΔΔGbind values in the computational alanine scanning (Supporting Information Fig. S12, SI-1). Of these, we excluded Q130 from further consideration since the putative hydrogen bond with yR40 is expected to be weaker than a salt bridge of yR40 with either D128 or E133. Moreover, among the 1,117 RNase III ortholog
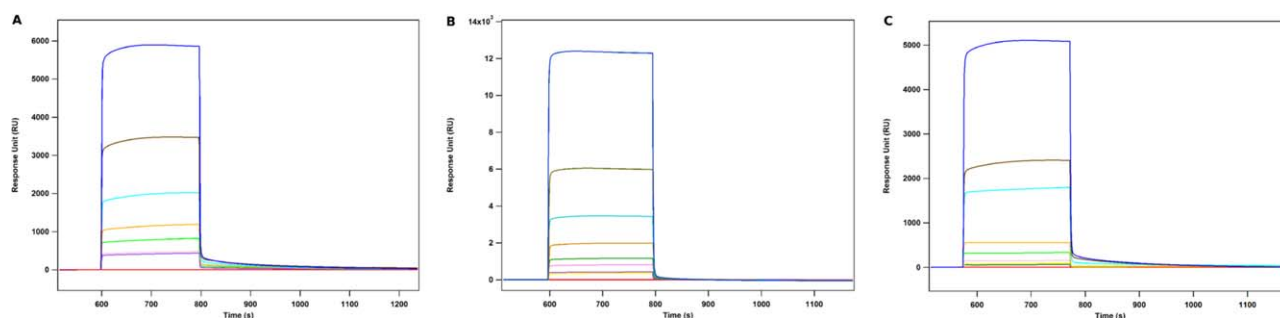
Figure 4

SPR analysis of the interaction of *Ec*-YmdB and *Ec*-RNase III. H6-YmdB and RNase III (with H6-tag removed) were purified as described in Supporting Information SI-3. H6-YmdB (50 n*M*) was immobilized on the NTA chip and subjected to a titration interaction analysis with injected RNase III, as described in Materials and Methods, and Supporting Information SI-3. The figures display the portion of the sensograms showing the association (RNase III injection) and dissociation (buffer injection) for a representative experiment. (**a**) Wild-type YmdB interaction with wild-type RNase III; the RNase III concentrations are 0 n*M* (red trace – buffer only), 5, 10, 25, 50, 100, 200, and 400 n*M* (blue trace). (**b**) R40A YmdB mutant interaction with wild-type RNase III; the RNase III concentrations used were the same as in (a), plus an additional experiment with 800 n*M* RNase III. (**c**) Wild-type YmdB interaction with the D128A/D128′A RNase III mutant. The RNase III concentrations used were: 0, 2, 5, 10, 20, 40, 80, 160, and 320 n*M*. Data were analyzed as described in Supporting Information SI-3. Sensogram traces were enhanced using Igor6. [Color figure can be viewed in the online issue, which is available at wileyonlinelibrary.com.]

sequences, Q130 is significantly less conserved (7.4%) than D128 (14.2%) or E133 (14.4%) [Fig. 3(A) and Supporting Information Fig. S32, SI-1]. D128 was chosen over E133 because (i) the interfacial frequency of D128 averaged over all the restrained docking poses (99%) is higher than that of E133 (64%); (ii) the (average) SASA buried on complex formation for D128 (40.7 Å^2) is larger than for E133 (25.1 Å^2); (iii) E133 is substituted by R or K (with 38.0% and 13.5% probability, respectively) in a number of RNase III orthologs [Fig. 3(A)]; and (iv) aspartic acid is a more frequent hot spot than glutamic acid.[65] Moreover, analysis of the D128A mutation would assess the functional importance of the predicted D128-Q130 hydrogen bond that spans the Ec-RNase III dimer interface [Fig. 2(C) and Supporting Information Fig. S23C, SI-1]. Taking all these factors together, we deemed D128 as a better candidate than E133 for experimental analysis.

The kinetic and thermodynamic parameters of the YmdB-RNase III interaction and the effect of the yR40A and D128A mutations were determined using SPR. YmdB was the immobilized species, and Ec-RNase III (with H6-tag removed) was the injected analyte. A sensogram of an RNase III titration experiment (performed at room temperature in pH 7.5 buffer containing 150 m*M* NaCl) is shown in Figure 4(A). The rate constants for complex formation and breakdown (k_a and k_d, respectively), and the equilibrium dissociation constant K_D (k_d/k_a) are provided in Table II. The k_a of 1×10^5 M^{-1}s^{-1} indicates a relatively rapid binding process, with the stability of the formed complex reflected in a k_d of 6.1×10^{-3} s^{-1}. The K_D of 61 n*M* corresponds to a free energy change on complex formation of −9.9 kcal/mol, and is consistent with a reversible bimolecular interaction.

An RNase III titration experiment was performed with the *Ec*-YmdB R40A mutant as the immobilized species [Fig. 4(B)]. The kinetic and thermodynamic parameters (Table II) reveal a significantly destabilized complex, with a K_D (1.1 μ*M*) that is 20-fold greater than the K_D for the wt/wt complex (61 n*M*). This difference ($\Delta\Delta G^{SPR} = +1.8$ kcal/mol) reflects the loss of a stabilizing interaction provided by the R40 side-chain (Table II). This is comparable to the values predicted by the computational analysis ($\Delta\Delta G^{FoldX} = +2.3$ kcal/mol, and $\Delta\Delta G^{Robetta} = +2.5$ kcal/mol), and accounts for 18% of the total free energy change on complex formation. The yR40A mutation causes a $\sim$10^3-fold decrease in the k_a value and a $\sim$60-fold decrease in the k_d value. Thus, the mutation significantly slows formation of the complex, as well as having a moderate slowing effect on complex dissociation. It is therefore likely that the R40 side-chain engages in specific local interactions that serve to stabilize the YmdB-RNase III complex.

The effect of the *Ec*-RNase III D128A/D128′A double mutation on complex formation and stability also was examined [Fig. 4(C)]. The results (see Table II) indicate a destabilized complex, as reflected in a K_D (5.8 μ*M*) that is $\sim$90-fold greater than the K_D of the wt/wt complex (61 n*M*). The experimental change in binding free energy ($\Delta\Delta G^{SPR} = +2.7$ kcal/mol) is greater than the calculated values ($\Delta\Delta G^{FoldX} = +1.5$ kcal/mol and $\Delta\Delta G^{Robetta} = +0.4$ kcal/mol). This difference can be explained in part by considering the limitations of the additivity approximation used to estimate the $\Delta\Delta G_{bind}$ of the mutant/mutant homodimer (see Materials and Methods); the value reported here for the D128A/D128A′ mutant is expected to be a lower limit of the actual value (see SI-1). The D128A/D128A′ mutation has only a

Table II
Kinetic and Thermodynamic Values for the YmdB-RNase III Interaction, and the Effect of Specific Mutations[a]

YmdB	RNase III	k_a (M^{-1}s^{-1})[b]	k_d (s^{-1})[b]	K_D (nM)	ΔG^{SPR} (kcal/mol)	$\Delta\Delta G^{SPR}$ (kcal/mol)	$\Delta\Delta G^{FoldX}$ (kcal/mol)[c]	$\Delta\Delta G^{Robetta}$ (kcal/mol)[#]
WT	WT	1.0×10^5	6.1×10^{-3}	61	−9.9	–	–	–
R40A	WT	59.1	6.7×10^{-5}	1100	−8.1	+1.8	+2.3	+2.5
WT	D128A/D128′A	6.4×10^4	0.37	5800	−7.2	+2.7	+1.5	+0.4

[a]Proteins were purified as described in Supporting Information SI-3. Measurements were performed at room temperature in a pH 7.5 buffer containing 150 mM NaCl (see Supporting Information SI-3).
[b]The χ^2 values for the global fits ranged from 1.1 to 2.2.
[c]An ensemble average was calculated over all the representative structures for the three restrained dockings [see Eq. (3) in Supporting Information SI-1]. The standard deviation of the FoldX values is 0.8 kcal/mol for the R40A YmdB mutant, and 0.3 kcal/mol for the D128A/D128′A RNase III double mutant. The standard deviation of the Robetta values is 0.3 and 0.2 kcal/mol, respectively. The value for the D128A/D128′A double mutant was approximated as the sum of the values calculated for the two heterodimer forms: D128A/WT and WT/D128′A [see Eq. (2) in Supporting Information SI-1].

minor effect on the association rate constant, but causes a ~100-fold increase in the dissociation rate constant (Table II). This behavior is qualitatively different than that observed with the yR40A mutation, which affects both the binding and dissociation events. The larger K_D value compared with that conferred by the yR40A mutation indicates that the D128A/D128′A mutation exerts a nonequivalent impact on complex stability. CD spectroscopic analysis reveals a qualitative difference in the spectrum of the D128A/D128′A mutant compared with that of wild-type protein (Supporting Information Fig. S1B, SI-4), indicating a mutation-induced secondary structure alteration. In contrast, the yR40A and wild-type YmdB spectra are essentially identical (Supporting Information Fig. S1A, SI-4). Since the computational alanine scanning analysis assumes that there are no significant structural changes on mutation, this would provide another source of the difference between the calculated and experimental $\Delta\Delta G_{bind}$ values for the YmdB-D128A/D128′A mutant complex. The enzymatic activity of the D128A/D128′A RNase III mutant was examined in an *in vitro* assay of RNA cleavage, using a model substrate. A time course assay performed under conditions of substrate excess reveals that the D128A/D128′A mutation significantly impairs RNase III catalytic activity (Supporting Information Fig. S1, SI-4). The implications of these findings on the YmdB-RNase III interaction, and potential regulatory mechanisms are discussed below.

DISCUSSION

We have combined computation and experimentation to investigate the interaction between RNase III and the macrodomain protein, YmdB. Docking calculations show that YmdB binds the homodimeric nuclease to form a 1:1 complex that is stabilized by contacts with the RNase III domain (RIIID), specifically within the region comprising residues 120-140. The RIIID recognition site is positioned at the RIIID-RIIID′ interface, on the surface opposite to the catalytic valley. The RIIID-YmdB-RIIID′

complex also shows that YmdB binding to RNase III can occur in the absence of any major structural rearrangement in either protein, including disruption of the RNase III homodimer. SPR analysis reveals a marked stability of the complex, and is consistent with the observations that an RNase III-YmdB complex can be directly isolated from *E. coli* cells using gentle lysis and affinity purification,[66] or isolated by bead-based affinity centrifugation following combination of the purified proteins.[13] Based on the effect of specific mutations that disrupt a predicted conserved interaction (see below), we believe that the modeled complex contains key features of the actual complex.

Kim *et al.* proposed that YmdB binding to RNase III creates a catalytically inactive heterodimer, in which an RNase III subunit is exchanged for a YmdB polypeptide.[13] This proposal was based on an observed reduction in an RNase III intersubunit covalent crosslink and the concomitant appearance of an RNase III-YmdB crosslink, following addition of YmdB and crosslinking agent. The computational modeling suggests an alternative explanation of the crosslinking results. Specifically, the region of the RIIID involved in YmdB binding includes the surface residue K134 (see Supporting Information Fig. S6B, SI-1). In the absence of YmdB, the K134 side-chain could be a target for reaction by the amine-specific reagent (disuccinimidyl suberate, DSS) used in the Kim et al. study.[13] The K134 and K134′ residues are within ~19 Å of each other, and could participate in an intersubunit crosslink since the maximum Cβ-Cβ distance cutoff for DSS crosslinking is 22.4 Å.[67] Binding of YmdB could block RNase III subunit crosslinking by sequestering K134 and/or K134′, and also create the opportunity for a YmdB-RNase III crosslink. However, the computational approaches used cannot strictly rule out formation of an RNase III-YmdB heterodimer, and the modeled complex could formally represent an intermediate in the heterodimer formation pathway.

The modeled RNase III-YmdB complex comprises a diverse structural ensemble (Supporting Information Figs. S9–S11, SI-1). The heterogeneity may be due to the limited data available to delimit the interacting surfaces

in the restrained docking calculations, resulting in a less well-defined structure of the complex. Alternatively, the docking solutions may capture some of the intermediate configurations formed during the initial interaction of the proteins (that is, encounter complexes).[68,69] An intriguing additional possibility is that the heterogeneity reflects an intrinsic structural disorder of the complex, due to the dynamic nature of the interactions. If so, the YmdB-RNase III complex may be similar to other well-documented "fuzzy" complexes.[70–72]

Kim et al. reported that Ec-YmdB also can affect the catalytic activity of S. coelicolor (Sc) RNase III, suggesting a conservation of the interaction. In this regard, the modeled E. coli YmdB-RNase III interface involves fully conserved (yR40) or partially conserved (D128, Q130, and E133) residues in the two proteins. For Ec-RNase III the primary recognition determinants are D128 and Q130 (located in the short loop that connects α-helices 6 and 7) and E133 (in helix α7). Sequence and structural alignments reveal that the loop is variable in length and sequence, but contains at least one acidic side chain. Despite the variability in the number and position of the acidic residues, the negatively-charged "pocket" appears to be a conserved feature of RNase III orthologs, as shown in representative electrostatic potential maps[73] (Supporting Information Fig. S14, SI-1). D128, Q130, and E133 are located directly at the RIIID-RIIID' subunit interface; thus, the RNase III homodimer would contain two YmdB recognition pockets, in close proximity, and across the interface. yR40 may bind to either the RIIID or the RIIID' pocket, or dynamically interact with both pockets. Thus, from a statistical standpoint, the three available options for recognition could enhance complex formation. However, the modeling does not support the possibility of a 2:1 complex in which a YmdB polypeptide binds to each pocket (RIIID-YmdB-YmdB-RIIID'), as this would impose severe steric overlap due to the proximity of the two recognition pockets.

YmdB residue R40 is a prominent element of the modeled complex [see Fig. 2(A)], as it sequesters the largest solvent accessible surface area (ΔSASA = 83–198 Å^2) on binding to the RNase III recognition pocket [see Fig. 2(C)]. SPR analysis reveals a significant energetic contribution of yR40 to complex stability, and the yR40A mutation causes a $\sim$10^3-fold decrease in the association rate constant, which may be attributed to the loss of the electrostatic interaction with the negatively charged pocket. Interestingly, the mutation also causes a $\sim$60-fold decrease in the dissociation rate constant. This does not have an obvious explanation, but could reflect the creation of alternative interactions (for example, involving yH39; see Table I, and Supporting Information Table SII and SI-1) that could retard complex breakdown. According to the "anchor-latch" model of Camacho and coworkers,[74] the formation of protein-protein complexes can involve the interaction of a specific surface residue (the "anchor"–usually Arg, Lys, or an aromatic residue) of the smaller protein with a binding pocket in the larger protein. The anchor residue is a primary contributor to the binding energy of the complex, and its mutation can have a dominant effect on the rate of association.[74] It is therefore tempting to speculate that yR40 is an anchor residue and primary recognition determinant.

The RNase III D128A/D128'A mutation has a greater effect on complex stability and has a qualitatively different effect on the kinetics of complex formation, compared to the yR40A mutation. Here, destabilization of the complex reflects a $\sim$100-fold increase in the dissociation rate constant, but an essentially unchanged association rate constant. To explain the latter observation, the adjacent E133 side-chain may provide an alternative, energetically equivalent electrostatic partner for yR40. However, the mutant RNase III pocket would have a reduced negative charge, and would not provide an optimal electrostatic environment for yR40. Significantly, the D128A/D128'A mutation also alters RNase III secondary structure (see Supporting Information Fig. S1B, SI-4). Thus, besides removing the predicted yR40 interaction, the mutation may indirectly disrupt additional interactions important for stabilizing the complex. The cause of the inhibitory effect of the D128A/D128'A mutation on catalytic activity is unclear, but suggests that the RIIID recognition pocket is important, most likely in an indirect manner, for binding and/or cleavage of substrate (see also below).

The structure of the RIIID-YmdB-RIIID' complex does not directly suggest a mechanism of regulation of RNase III by YmdB. Any feasible mechanism would need to incorporate the observation that inhibition is dependent on YmdB levels. If it is assumed that the RIIID-YmdB-RIIID' complex is present under normal growth conditions (reflecting a need for both proteins), without an inhibitory influence of YmdB, then an additional binding site must be considered. As YmdB levels increase, the additional site would be occupied, forming a 2:1 complex; this would be consistent with the observation by Kim et al.[13] that the threshold YmdB/RNase III ratio required for inhibition is >1:1. The RNase III-YmdB interaction would then be similar to other protein-protein complexes, in which the stoichiometry changes with the concentration of one of the partners.[36] Moreover, the occurrence of two binding sites, whose occupancy has different functional effects has been described for other complexes.[75,76] A second site with inhibitory potential is suggested by the blind docking, revealing poses in which YmdB interacts with the dsRBDs and bound dsRNA (see clusters 2 and 5 in Fig. 2). The presence of YmdB in the second site could (i) block substrate binding, (ii) trap a pre-catalytic complex in an unreactive state, or (iii) hinder product release. In this regard, under conditions where catalysis is

prevented, RNase III appears to bind substrate more tightly in the presence of YmdB.[13] The SPR analysis was not able to detect complexes containing multiple copies of YmdB, since YmdB was the surface-attached species. Thus, other approaches will be necessary to detect higher-order complexes. We also note that YmdB interaction with the dsRBD and dsRNA also would be compatible with a complex involving a noncleavable RNA, instead of substrate or product RNA proposed above. RNase III binding to RNA without concomitant cleavage has been implicated in gene regulation,[4,77–79] and the presence of YmdB may stabilize such a complex, with potential gene-regulatory effects.

How YmdB affects RNase III catalytic activity *in vitro* remains unclear. Makarov and Apirion[80] first described YmdB inhibition of RNase III cleavage of RNA *in vitro* (although in that study the ∼18 kDa inhibitory polypeptide had not been identified as YmdB). The reaction employed the nonphysiological conditions of low salt (12 mM NH$_4^+$) and Mn^{2+} ion (0.1 mM). In addition, the RNA used ("p10Sa RNA") is not a natural substrate for RNase III, and is only efficiently cleaved in the nonphysiological conditions described above. It is therefore possible that the use of an otherwise unreactive substrate in a nonphysiological buffer could significantly accentuate an otherwise weak inhibitory action of YmdB. In contrast, Kim *et al.* demonstrated only modest inhibition, using the same nonphysiological conditions, but with an physiological substrate, R1.1 RNA.[13] We found no significant inhibition by YmdB of RNase III action on R1.1 RNA, using physiologically relevant conditions (5 mM Mg^{2+}, 150 mM NaCl, pH 7.5; S. Paudyal, unpublished experiments). We therefore believe that additional factors are necessary to reconstruct *in vitro* the observed *in vivo* regulatory action of YmdB. In this regard, elevated YmdB levels are necessary but not sufficient to confer regulation, since *in vivo* conditions, such as nutrient starvation, cause an increase in YmdB levels without significantly diminishing RNase III activity.[13] Binding of ADPR or related metabolite to the YmdB macrodomain is one possibility, since several of the YmdB residues predicted to be at the RNase III interface (including G32, G124, V125, Y126, and Y159) are also near the ADPR binding site[16]. However, inclusion of ADPR at concentrations (>1 mM) sufficient to saturate the binding site does not promote inhibition (S. Paudyal, unpublished experiments). Further analyses of YmdB and identification of additional factors are needed to better understand the role of this conserved macrodomain protein in RNase III regulation.

ACKNOWLEDGMENTS

REFERENCES

1. Deutscher MP. Degradation of RNA in bacteria: comparison of mRNA and stable RNA. Nucleic Acids Res 2006;34:659–666.
2. Condon C. Maturation and degradation of RNA in bacteria. Curr Opin Microbiol 2007;10:271–278.
3. Arraiano CM, Andrade JM, Domingues S, Guinote IB, Malecki M, Matos RG, Moreira RN, Pobre V, Reis FP, Saramago M, Silva IJ, Viegas SC. The critical role of RNA processing and degradation in the control of gene expression. FEMS Microbiol Rev 2010;34:883–923.
4. Court DL, Gan J, Liang Y-H, Shaw GX, Tropea JE, Costantino N, Waugh DS, Ji X. RNase III: genetics and function; structure and mechanism. Annu Rev Genet 2013;47:405–431.
5. Nicholson AW. Ribonuclease III mechanisms of double-stranded RNA cleavage. WIREs RNA 2014;5:31–48.
6. Deutscher MP. Maturation and degradation of ribosomal RNA in bacteria. Prog Mol Biol Transl Sci 2009;85:369–391.
7. Régnier P, Grunberg-Manago M. RNase III cleavages in non-coding leaders of Escherichia coli transcripts control mRNA stability and genetic expression. Biochimie 1990;72:825–8d34.
8. Nicholson AW. Ribonuclease III and the role of double-stranded RNA processing in bacterial systems. In: Nicholson AW, editor. Ribonucleases (Nucleic Acids and Molecular Biology 26). Berlin Heidelberg: Springer-Verlag; 2011. p 269−297.
9. Chen SM, Takiff HE, Barber AM, Dubois GC, Bardwell JC, Court DL. Expression and characterization of RNase III and era proteins. Products of the rnc operon of Escherichia coli. J Biol Chem 1990; 265:2888–2895.
10. Bardwell JCA, Régnier P, Chen S-M, Nakamura Y, Grunberg-Manago MP, Court DL. Autoregulation of RNase III operon by mRNA processing. EMBO J 1989;8:3401–3407.
11. Matsunaga J, Simons EL, Simons RW. RNase III autoregulation: structure and function of rncO, the post-transcriptional 'operator'. RNA 1996;2:1228–1240.
12. Mayer JE, Schweiger M. RNase III is positively regulated by T7 protein kinase. J Biol Chem 1983;258:5340–5343.
13. Kim K-S, Manasherob R, Cohen SN. YmdB: a stress-responsive ribonuclease-binding regulator of E. coli RNase III activity. Genes Dev 2008;22:3497–3508.
14. Karras GI, Kustatscher G, Buhecha HR, Allen MD, Pugieux C, Sait F, Bycroft M, Ladurner AG. The macro domain is an ADP-ribose binding module. EMBO J 2005;24:1911–1920.
15. Han W, Li X, Fu X. The macro domain protein family: structure, functions, and their potential therapeutic implications. Mutat Res 2011;727:86–103.
16. Chen D, Vollmar M, Rossi MN, Phillips C, Kraehenbuehl R, Slade D, Mehrotra PV, von Delft F, Crosthwaite SK, Gileadi O, Denu JM, Ahel I. Identification of macrodomain proteins as novel O-acetyl-ADP-ribose deacetylases. J Biol Chem 2011;286:13261–13271.
17. Zhao K, Chai X, Marmorstein R. Structure and substrate binding properties of cobB, a Sir2 homolog protein deacetylase from Escherichia coli. J Mol Biol 2004;337:731–741.
18. Kim T, Lee J, Kim K-S. Escherichia coli YmdB regulates biofilm formation independently of its role as an RNase III modulator. BMC Microbiol 2013;13:266
19. Amarasinghe AK, Calin-Jageman I, Harmouch A, Sun W, Nicholson AW. Escherichia coli ribonuclease III: affinity purification of hexahistidine-tagged enzyme and assays for substrate binding and cleavage. Methods Enzymol 2001;342:143–158.
20. Gan J, Shaw G, Tropea JE, Waugh DS, Court DL, Ji X. A stepwise model for double-stranded RNA processing by ribonuclease III. Mol Microbiol 2008;67:143–154.

21. Gan J, Tropea JE, Austin BP, Court DL, Waugh DS, Ji X. Intermediate states of ribonuclease III in complex with double-stranded RNA. Structure 2005;13:1435–1442.

22. Finn RD, Clements J, Eddy SR. HMMER web server: interactive sequence similarity searching. Nucleic Acids Res 2011;39:W29–W37.

23. Robert X, Gouet P. Deciphering key features in protein structures with the new ENDscript Server. Nucleic Acids Res 2014;42:W320–W324.

24. Buchan DWA, Minneci F, Nugent TCO, Bryson K, Jones DT. Scalable webservices for the PSIPRED protein analysis workbench. Nucleic Acids Res 2013;41:W349–W357.

25. Baker D, Sali A. Protein structure prediction and structural genomics. Science 2001;294:93–96.

26. Eramian D, Eswar N, Shen M-Y, Sali A. How well can the accuracy of comparative protein structure models be predicted? Protein Sci 2008;17:1881–1893.

27. Sali A, Blundell TL. Comparative protein modelling by satisfaction of spatial restraints. J Mol Biol 1993;234:779–815.

28. Fiser A, Do RKG, Sali A. Modeling of loops in protein structures. Protein Sci 2000;9:1753–1773.

29. Lindahl E, Hess B, Van Der Spoel D. GROMACS 3.0: a package for molecular simulation and trajectory analysis. Mol Model Annu 2001;7:306–317.

30. Daura X, Gademann K, Jaun B, Seebach D, van Gunsteren WF, Mark AE. Peptide folding: when simulation meets experiment. Angew Chem Int Ed 1999;38:236–240.

31. Domínguez C, Boelens R, Bonvin AMJJ. HADDOCK: a protein-protein docking approach based on biochemical or biophysical information. J Am Chem Soc 2003;125:1731–1737.

32. De Vries SJ, van Dijk AD, Krzeminski M, van Dijk M, Thureau A, Hsu V, Wassenaar T, Bonvin AMJJ. HADDOCK versus HADDOCK: new features and performance of HADDOCK2.0 on the CAPRI targets. Proteins 2007;69:726–733.

33. Brünger AT, Adams PD, Clore GM, DeLano WL, Gros P, Grosse-Kunstleve RW, Jiang JS, Kuszewski J, Nilges M, Pannu NS, Read RJ, Rice LM, Simonson T, Warren GL. Crystallography and NMR system: a new software suite for macromolecular structure determination. Acta Crystallogr D Biol Crystallogr 1998;54:905–921.

34. Brünger AT. Version 1.2 of the crystallography and NMR system. Nat Protoc 2007;2:2728–2733.

35. Rodrigues JP, Melquiond AS, Karaca E, Trellet M, van Dijk M, van Zundert GC, Schmitz C, de Vries SJ, Bordogna A, Bonati L, Kastritis PL, Bonvin AM. Defining the limits of homology modeling in information-driven protein docking. Proteins 2013;81:2119–2128.

36. Volkov AN, Ferrari D, Worrall JAR, Bonvin AMJJ, Ubbink M. The orientations of cytochrome c in the highly dynamic complex with cytochrome b5 visualized by NMR and docking using HADDOCK. Protein Sci 2005;14:799–811.

37. Humphrey W, Dalke A, Schulten K. VMD: visual molecular dynamics. J Mol Graph 1996;14:33–38.

38. Cohen J, Arkhipov A, Braun R, Schulten K. Imaging the migration pathways for O_2, CO, NO, and Xe inside myoglobin. Biophys J 2006;91:1844–1857.

39. Fernández-Recio J, Totrov M, Abagyan R. Identification of protein–protein interaction sites from docking energy landscapes. J Mol Biol 2004;335:843–865.

40. Medina M, Abagyan R, Gómez-Moreno C, Fernández-Recio J. Docking analysis of transient complexes: interaction of ferredoxin-$NADP^+$ reductase with ferredoxin and flavodoxin. Proteins 2008;72:848–862.

41. De Vries SJ, van Dijk ADJ, Bonvin AMJJ. WHISCY: what information does surface conservation yield? Application to data-driven docking. Proteins 2006;63:479–489.

42. Movshovitz-Attias D, London N, Schueler-Furman O. On the use of structural templates for high-resolution docking. Proteins 2010;78:1939–1949.

43. Tanner DE, Chan K-Y, Phillips JC, Schulten K. Parallel generalized born implicit solvent calculations with NAMD. J Chem Theory Comput 2011;7:3635–3642.

44. Phillips JC, Braun R, Wang W, Gumbart J, Tajkhorshid E, Villa E, Chipot C, Skeel RD, Kale L, Schulten K. Scalable molecular dynamics with NAMD. J Comput Chem 2005;26:1781–1802.

45. Cornell WD, Cieplak P, Bayly CI, Gould IR, Merz KM, Ferguson DM, Spellmeyer DC, Fox T, Caldwell JW, Kollman PA. A second generation force field for the simulation of proteins, nucleic acids, and organic molecules. J Am Chem Soc 1995;117:5179–5197.

46. Pérez A, Marchán I, Svozil D, Sponer J, Cheatham IIITE, Laughton CA, Orozco M. Refinement of the AMBER force field for nucleic acids: improving the description of α/γ conformers. Biophys J 2007;92:3817–3829.

47. Åqvist J. Ion-water interaction potentials derived from free energy perturbation simulations. J Phys Chem 1990;94:8021–8024.

48. Allnér O, Nilsson L, Villa A. Magnesium ion–water coordination and exchange in biomolecular simulations. J Chem Theory Comput 2012;8:1493–1502.

49. Chen VB, Arendall WB, Headd JJ, Keedy DA, Immormino RM, Kapral GJ, Murray LW, Richardson JS, Richardson DC. MolProbity: all-atom structure validation for macromolecular crystallography. Acta Crystallogr D Biol Crystallogr 2009;66:12–21.

50. Durrant JD, McCammon JA. BINANA: a novel algorithm for ligand-binding characterization. J Mol Graph Model 2011;29:888–893.

51. Schymkowitz J, Borg J, Stricher F, Nys R, Rousseau F, Serrano L. The FoldX web server: an online force field. Nucleic Acids Res 2005;33:W382–W388.

52. Kortemme T, Kim DE, Baker D. Computational alanine scanning of protein-protein interfaces. Sci STKE 2004;2004:pl2.

53. Grosdidier S, Fernández-Recio J. Identification of hot-spot residues in protein-protein interactions by computational docking. BMC Bioinformatics 2008;9:447

54. Serrano L, Horovitz A, Avron B, Bycroft M, Fersht AR. Estimating the contribution of engineered surface electrostatic interactions to protein stability by using double-mutant cycles. Biochemistry 1990;29:9343–9352.

55. Jakobi S, Nguyen TXP, Debaene F, Metz A, Sanglier-Cianférani S, Reuter K, Klebe G. Hot-spot analysis to dissect the functional protein–protein interface of a tRNA-modifying enzyme. Proteins 2014;82:2713–2732.

56. Altschul SF, Madden TL, Schäffer AA, Zhang J, Zhang Z, Miller W, Lipman DJ. Gapped BLAST and PSI-BLAST: a new generation of protein database search programs. Nucleic Acids Res 1997;25:3389–3402.

57. Sievers F, Wilm A, Dineen D, Gibson TJ, Karplus K, Li W, Lopez R, McWilliam H, Remmert M, Soding J, Thompson JD, Higgins DG. Fast, scalable generation of high-quality protein multiple sequence alignments using clustal omega. Mol Syst Biol 2011;7:539

58. Schneider TD, Stephens RM. Sequence logos: a new way to display consensus sequences. Nucleic Acids Res 1990;18:6097–6100.

59. Crooks GE, Hon G, Chandonia J-M, Brenner SE. WebLogo: a sequence logo generator. Genome Res 2004;14:1188–1190.

60. Akey DL, Berger JM. Structure of the nuclease domain of ribonuclease III from M. tuberculosis at 2.1 Å. Protein Sci 2005;14:2744–2750.

61. Pieper U, Eswar N, Webb BM, Eramian D, Kelly L, Barkan DT, Carter H, Mankoo P, Karchin R, Marti-Renom MA, Davis FP, Sali A. MODBASE, a database of annotated comparative protein structure models and associated resources. Nucleic Acids Res 2009;37:D347–D354.

62. Raju SG, Barber AF, LeBard DN, Klein ML, Carnevale V. Exploring volatile general anesthetic binding to a closed membrane-bound bacterial voltage-gated sodium channel via computation. PLoS Comput Biol 2013;9:e1003090

63. Van Dijk ADJ, De Vries SJ, Dominguez C, Chen H, Zhou H-X, Bonvin AMJJ. Data-driven docking: HADDOCK's adventures in CAPRI. Proteins 2005;60:232–238.

64. Meireles LMC, Dömling AS, Camacho CJ. ANCHOR: a web server and database for analysis of protein–protein interaction binding pockets for drug discovery. Nucleic Acids Res 2010;38:W407–W411.

65. Bogan AA, Thorn KS. Anatomy of hot spots in protein interfaces. J Mol Biol 1998;280:1–9.

66. Hu P, Janga SC, Babu M, Díaz-Mejía JJ, Butl G, Yang W, Pogoutse O, Guo X, Phanse S, Wong P, Chandran S, Christopoulos C, Nazarians-Armavil A, Nasseri NK, Musso G, Ali M, Nazemof N, Eroukova V, Golshani A, Paccanaro A, Greenblatt JF, Moreno-Hagelsieb G, Emili A. Global functional atlas of Escherichia coli encompassing previously uncharacterized proteins. PLoS Biol 2009; 7:e1000096.

67. Kahraman A, Malmström L, Aebersold R. Xwalk: computing and visualizing distances in cross-linking experiments. Bioinformatics 2011;27:2163–2164.

68. Ubbink M. The courtship of proteins: understanding the encounter complex. FEBS Lett 2009;583:1060–1066.

69. Ubbink M. Dynamics in transient complexes of redox proteins. Biochem Soc Trans 2012;40:415–418.

70. Tompa P, Fuxreiter M. Fuzzy complexes: polymorphism and structural disorder in protein–protein interactions. Trends Biochem Sci 2008;33:2–8.

71. Welch GR. 'Fuzzines' in the cellular interactome: a historical perspective. Adv Exp Med Biol 2012;725:184–190.

72. Zhang L, Buck M. Molecular simulations of a dynamic protein complex: role of salt-bridges and polar interactions in configurational transitions. Biophys J 2013;105:2412–2417.

73. Baker NA, Sept D, Joseph S, Holst MJ, McCammon JA. Electrostatics of nanosystems: application to microtubules and the ribosome. Proc Natl Acad Sci 2001;98:10037–10041.

74. Rajamani D, Thiel S, Vajda S, Camacho CJ. Anchor residues in protein–protein interactions. Proc Natl Acad Sci USA 2004;101:11287–11292.

75. Tompa P, Szasz C, Buday L. Structural disorder throws new light on moonlighting. Trends Biochem Sci 2005;30:484–489.

76. Copley SD. Moonlighting is mainstream: paradigm adjustment required. BioEssays 2012;34:578–588.

77. Ji X. Structural basis for non-catalytic and catalytic activities of ribonuclease III. Acta Cryst D Biol Crystallogr 2006;62:933–940.

78. Pertzev AV, Nicholson AW. Characterization of RNA sequence determinants and antideterminants of processing reactivity for a minimal substrate of Escherichia coli ribonuclease III. Nucleic Acids Res 2006;34:3708−3721.

79. Gatewood ML, Bralley P, Weil MR, Jones GH. RNA-seq and RNA immunoprecipitation analyses of the transcriptome of Streptomyces coelicolor identify substrates for RNase III. J Bacteriol 2012;194: 2228–2237.

80. Makarov EM, Apirion D. 10Sa RNA: processing by and inhibition of RNase III. Biochem Int 1992;26:1115–1124.